

ADP-15-25/T927
DESY 15-154
Edinburgh 2015/19
Liverpool LTH 1054
August 24, 2015

Wilson flow and scale setting from lattice QCD

V. G. Bornyakov^a, R. Horsley^b, R. Hudspith^c, Y. Nakamura^d,
H. Perlt^e, D. Pleiter^f, P. E. L. Rakow^g, G. Schierholz^h,
A. Schiller^e, H. Stübenⁱ and J. M. Zanotti^j

– QCDSF-UKQCD Collaboration –

^a Institute for High Energy Physics, Protvino,
142281 Protvino, Russia,
Institute of Theoretical and Experimental Physics, Moscow,
117259 Moscow, Russia,
School of Biomedicine, Far Eastern Federal University,
690950 Vladivostok, Russia

^b School of Physics and Astronomy, University of Edinburgh,
Edinburgh EH9 3FD, UK

^c Department of Mathematics and Statistics, York University,
Toronto, ON Canada M3J 1P3

^d RIKEN Advanced Institute for Computational Science,
Kobe, Hyogo 650-0047, Japan

^e Institut für Theoretische Physik, Universität Leipzig,
04109 Leipzig, Germany

^f Jülich Supercomputing Centre, Forschungszentrum Jülich,
52425 Jülich, Germany,
Institut für Theoretische Physik, Universität Regensburg,
93040 Regensburg, Germany

^g Theoretical Physics Division, Department of Mathematical Sciences,
University of Liverpool, Liverpool L69 3BX, UK

^h Deutsches Elektronen-Synchrotron DESY,
22603 Hamburg, Germany

ⁱ Regionales Rechenzentrum, Universität Hamburg,
20146 Hamburg, Germany

^j CSSM, Department of Physics, University of Adelaide,
Adelaide SA 5005, Australia

Abstract

We give a determination of the phenomenological value of the Wilson (or gradient) flow scales t_0 and w_0 for $2 + 1$ flavours of dynamical quarks. The simulations are performed keeping the average quark mass constant, which allows the approach to the physical point to be made in a controlled manner. $O(a)$ improved clover fermions are used and together with four lattice spacings this allows the continuum extrapolation to be taken.

1 Introduction

Numerical lattice QCD simulations naturally determine dimensionless quantities such as mass ratios and matrix element ratios, however determining a physical value requires the introduction of a scale, usually taken from experiment. A hadron mass, such as the proton mass, or decay constant, such as the pion decay constant, are often used for this purpose. We discuss here setting the scale using flavour-singlet quantities, which in conjunction with simulations keeping the average quark mass constant allow $SU(3)$ flavour breaking expansions to be used. This is illustrated here using $2 + 1$ clover fermions, and a determination of the Wilson flow scales t_0 and w_0 is given. These are ‘secondary’ scales and are not experimentally accessible and thus they have to be matched to physical quantities. These flow scales are cheap to compute from lattice simulations (for example they do not require a knowledge of quark propagators) and accurate (for example they do not require a determination of the potential which requires the limit of a large distance). So once the phenomenological value of the flow scales is known the determination of physical values becomes more tractable.

Flow and flow variables were introduced by Lüscher, [1]. We follow him here, [2], in particular in our brief discussion of the t_0 scale. Flow represents a smoothing of the gauge fields. We denote the flow time by t , and the link variables at this time by $U_\mu(x, t) = \exp(iT^a \theta_\mu^a(x, t))$ which evolve according to

$$\frac{dU_\mu(x, t)}{dt} = iT^a \frac{\delta S_{\text{flow}}[U]}{\delta \theta_\mu^a(x, t)} U_\mu(x, t), \quad \text{with } U_\mu(x, 0) = U_\mu(x), \quad (1)$$

with $S_{\text{flow}}[U]$ being the flow action, which does not have to be the same as the action used to generate the gauge variable. (x is just the normal 4-dimensional Euclidean space-time.) Setting

$$F(t) \equiv t^2 \langle E(t) \rangle, \quad \text{where } E(t) = \frac{1}{4} F_{\mu\nu}^a{}^2(t), \quad (2)$$

then we define the t_0 scale by

$$F(t)|_{t=t_0(c)} = c. \quad (3)$$

Alternatively, [3] define the w_0 scale as

$$t \frac{d}{dt} F(t) \Big|_{t=w_0^2(c)} = c, \quad (4)$$

where in both definitions c is a constant, conventionally taken as $c = 0.3$. We require a value of c such that $a \ll \sqrt{8t_0} \ll L$, L being the lattice size and this value was found to be a suitable choice, [2]. Alternative suggestions have been made, see e.g. [4, 5].

In this article we shall give a determination of $\sqrt{t_0^{\text{exp}}}$ and w_0^{exp} . There have been several determinations for different numbers of flavours. These include quenched $n_f = 0$ or quenched, [5, 6]; $n_f = 2$, [7, 8]; $n_f = 2 + 1$, [9, 3, 10]; $n_f = 2 + 1 + 1$, [11, 12, 13]. We have also published preliminary results, [14].

The plan of this article is as follows. In section 2 we describe our method of approaching the physical quark mass starting from a point on the $SU(3)$ flavour symmetric line, [15, 16]. We also discuss the general property of singlet quantities, that they have a stationary point about this $SU(3)$ flavour symmetric line. Section 3 gives examples of singlet quantities both hadronic and gluonic (i.e. in this case t_0 and w_0) and also discusses their $SU(3)$ flavour breaking expansions. Section 4 first gives our lattice conventions, ensembles used and numerical values of the singlet quantities. This is followed by section 5 in which the $\sqrt{t_0}$ and w_0 scales are determined for several lattice spacings. In the next section, section 6 we take the continuum result to give the final result. Finally in section 7 we compare our result with other results for $n_f = 2 + 1$ flavours and give our conclusions.

2 Extrapolating flavour singlet quantities

We consider extrapolations to the physical point from a point on the $SU(3)$ flavour symmetric line keeping the average quark mass fixed, [15, 16],

$$\bar{m} = \frac{1}{3}(m_u + m_d + m_s) = \text{const.} \quad (5)$$

This means that as the pion mass tends downwards to its physical value, the kaon mass increases upwards to its physical value. (In particular the kaon mass is never larger than its physical value.) Possible scenarios are sketched in Fig. 1 for a path from a point on the $SU(3)$ flavour symmetric line to the physical point for the case of mass degenerate u and d quarks m_l , see eq. (12). (For non-mass degenerate u and d quarks we would have instead a plane.) Shown in Fig. 1 are the bare and renormalised quark masses for the case discussed here of clover fermions. (Because the singlet and non-singlet pieces renormalise differently the renormalised quark axes are not orthogonal to each other, as further discussed in [16]. For chiral fermions this would not be the case.) In the left hand panel one

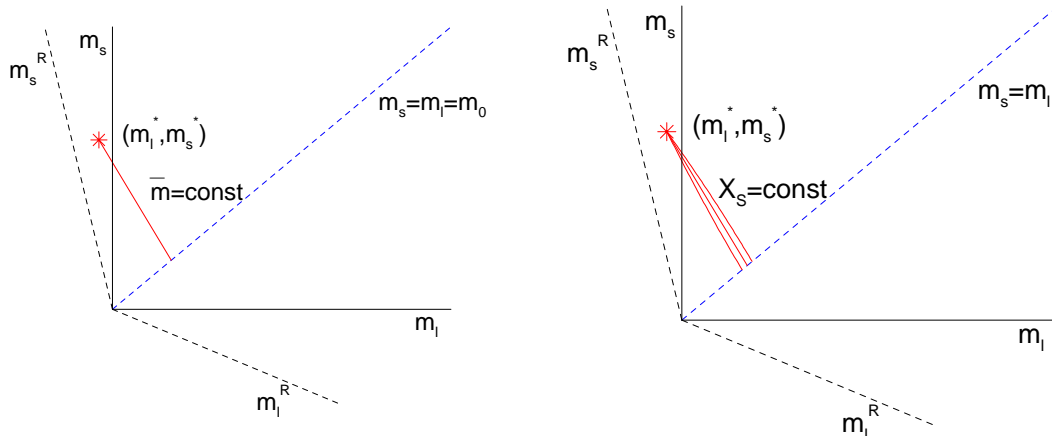


Figure 1: Possible scenarios for the path in the $(m_u = m_d \equiv) m_l - m_s$ plane. In the LH panel $\bar{m} = \text{const.}$, while in the RH panel we hold other singlet quantities constant.

common trajectory is sufficient, while in the right hand panel it depends on the singlet quantity used, [16].

With the condition of eq. (5) flavour singlet quantities turn out to have a stationary point in the quark mass starting from a given point on the $SU(3)$ flavour symmetric line. As we shall see this potentially allows simpler extrapolations to the physical point. This property may be shown by considering small changes about a given point on the $SU(3)$ flavour symmetric line. Let $X_S(m_u, m_d, m_s)$ be a flavour singlet object i.e. X_S is invariant under the quark permutation symmetry between u , d and s . Then Taylor expanding X_S about a point m_0 on the $SU(3)$ flavour symmetric line $m_u = m_d = m_s = m_0 \equiv \bar{m}$,

$$m_q = \bar{m} + \delta m_q, \quad (6)$$

gives

$$\begin{aligned} & X_S(\bar{m} + \delta m_u, \bar{m} + \delta m_d, \bar{m} + \delta m_s) \\ &= X_S(\bar{m}, \bar{m}, \bar{m}) + \left. \frac{\partial X_S}{\partial m_u} \right|_0 \delta m_u + \left. \frac{\partial X_S}{\partial m_d} \right|_0 \delta m_d + \left. \frac{\partial X_S}{\partial m_s} \right|_0 \delta m_s + O((\delta m_q)^2). \end{aligned} \quad (7)$$

But on the symmetric line we have

$$\left. \frac{\partial X_S}{\partial m_u} \right|_0 = \left. \frac{\partial X_S}{\partial m_d} \right|_0 = \left. \frac{\partial X_S}{\partial m_s} \right|_0, \quad (8)$$

and on our chosen trajectory, eq. (5)

$$\delta m_u + \delta m_d + \delta m_s = 0, \quad (9)$$

which together imply that

$$X_S(\overline{m} + \delta m_u, \overline{m} + \delta m_d, \overline{m} + \delta m_s) = X_S(\overline{m}, \overline{m}, \overline{m}) + O((\delta m_q)^2). \quad (10)$$

In other words, the effect at first order of changing the strange quark mass is cancelled by the change in the light quark mass, so we know that X_S must have a stationary point on the $SU(3)$ flavour symmetric line.

Thus provided the quadratic terms in eq. (10) are small it will not matter which singlet quantity we use, all are equivalent to keeping $\overline{m} = \text{const.}$, the scenario of the left hand panel of Fig. 1.

3 Defining singlet quantities

We shall consider here hadronic singlet quantities, such as independent averages with respect to quark permutations of the pseudoscalar, vector and nucleon octets, [15, 16], and also gluonic quantities derived from the Wilson flow, [2, 3]. In particular we shall consider

$$\begin{aligned} X_\pi^2 &= \frac{1}{6}(M_{K^+}^2 + M_{K^0}^2 + M_{\pi^+}^2 + M_{\pi^0}^2 + M_{K^-}^2 + M_{\overline{K}^0}^2) = \frac{1}{3}(2M_K^2 + M_\pi^2) \\ X_\rho^2 &= \frac{1}{6}(M_{K^{*+}}^2 + M_{K^{*0}}^2 + M_{\rho^+}^2 + M_{\rho^0}^2 + M_{K^{*0}}^2 + M_{K^{*-}}^2) = \frac{1}{3}(2M_{K^*}^2 + M_\rho^2) \\ X_N^2 &= \frac{1}{6}(M_p^2 + M_n^2 + M_{\Sigma^+}^2 + M_{\Sigma^0}^2 + M_{\Sigma^-}^2 + M_{\Xi^0}^2 + M_{\Xi^-}^2) = \frac{1}{3}(M_N^2 + M_\Sigma^2 + M_\Xi^2) \\ X_{t_0}^2 &= 1/t_0 \\ X_{w_0}^2 &= 1/w_0^2. \end{aligned} \quad (11)$$

(The charge conjugate mesons have the same masses, at least for pure QCD. For example $M_{\pi^+} = M_{\pi^-}$, $M_{K^+} = M_{K^-}$ and $M_{K^0} = M_{\overline{K}^0}$, obviously no such similar result holds for the baryons.) The second expressions are the masses for mass degenerate u and d quarks,

$$m_u = m_d \equiv m_l. \quad (12)$$

Except for X_π^2 , which is naturally an average over quadratic masses, it does not matter whether we consider linear or quadratic averages – quadratic averages were found to give slightly better fits for heavy partially quenched masses (up to the charm quark); in the small quark mass range considered here this is less important. Note also that for the Wilson flow singlets we consider the inverse of the flow variable as then all singlet quantities have the same dimensions.

Other possibilities, as discussed in [16] include the further nucleon octet singlet

$$X_\Lambda^2 = \frac{1}{2}(M_{\Lambda^0}^2 + M_{\Sigma^0}^2) = \frac{1}{2}(M_\Lambda^2 + M_\Sigma^2), \quad (13)$$

and baryon decuplet singlets

$$\begin{aligned} X_\Delta^2 &= \frac{1}{3}(M_{\Delta^{++}}^2 + M_{\Delta^+}^2 + M_{\Omega^-}^2) = \frac{1}{3}(2M_\Delta^2 + M_\Omega^2) \\ X_{\Xi^*}^2 &= \frac{1}{6}(M_{\Delta^+}^2 + M_{\Delta^0}^2 + M_{\Sigma^{*+}}^2 + M_{\Sigma^{*0}}^2 + M_{\Xi^{*0}}^2 + M_{\Xi^{*-}}^2) = \frac{1}{3}(M_\Delta^2 + M_\Sigma^2 + M_\Xi^2) \\ X_{\Sigma^*}^2 &= M_{\Sigma^{*0}}^2 = M_{\Sigma^*}^2. \end{aligned} \quad (14)$$

Singlet quantity	GeV
X_π^{exp}	0.4126
X_ρ^{exp}	0.8562
X_N^{exp}	1.1610
X_Λ^{exp}	1.1548
X_Δ^{exp}	1.3944(12)
$X_{\Xi^*}^{\text{exp}}$	1.3837(1)
$X_{\Sigma^*}^{\text{exp}}$	1.3888(6)

Table 1: Experimental values for various singlet quantities, averaging over (masses)² (to 4 decimal places).

Further possibilities can be constructed from ‘fictitious’ particles, such as a ‘nucleon’, N_s , with three mass degenerate quarks at the strange quark mass. At the $SU(3)$ flavour symmetric points, all the baryon octet hadrons are mass degenerate (at least from a QCD perspective), so we expect that away from this point there is no (or very little) difference between X_N^2 and X_Λ^2 , i.e. $X_N = X_\Lambda$. The same argument holds for the various baryon decuplet possibilities, i.e. $X_\Delta = X_{\Xi^*} = X_{\Sigma^*}$.

How far does this extend? Let us consider the experimental (or phenomenological) singlet hadron mass results¹ as given in Table 1². It is seen that even after the extrapolation from the $SU(3)$ flavour line to the experimental point, then $X_N^{\text{exp}} \approx X_\Lambda^{\text{exp}}$ and $X_\Delta^{\text{exp}} \approx X_{\Xi^*}^{\text{exp}} \approx X_{\Sigma^*}^{\text{exp}}$ the worst discrepancy (between $X_{\Xi^*}^{\text{exp}}$ and $X_{\Sigma^*}^{\text{exp}}$) is only a fraction of a percent. This indicates that quite likely the X_S are constant over a large interval.

However as the baryon decuplet possibilities are numerically substantially noisier, we shall only use the baryon octet hadrons here.

An equivalent statement (for singlet quantities built from hadron masses) is found by considering the $SU(3)$ flavour breaking expansion. As discussed in [15, 16] we have for the octet mesons, $\pi^+(u\bar{d})$, $\pi^-(d\bar{u})$, $K^+(u\bar{s})$, $K^-(s\bar{u})$, $K^0(d\bar{s})$ and $\bar{K}^0(s\bar{d})$ not lying at the centre of the octet

$$M^2(a\bar{b}) = M_0^2 + \alpha_\pi(\delta m_a + \delta m_b) + O((\delta m_q)^2), \quad (15)$$

where a and b are u , d or s quarks. Similar results hold for the vector mesons. For the $p(uud)$, $n(duu)$, $\Sigma^+(uus)$, $\Sigma^-(dds)$, $\Xi^0(ssu)$, $\Xi^-(ssd)$ baryons on the outer

¹Only when necessary and for clarity do we distinguish between experimental and lattice masses – X_S^{exp} and X_S^{lat} respectively.

²As we are not considering mass differences, then the effect of electromagnetic effects is small, and so we can disregard them here. For example for the lightest particles – the pseudoscalar octet, the value given in Table 1 for X_π is to be compared with the value upon using Dashen’s theorem which gives 0.4116 GeV (see e.g. [19]). This is a $\lesssim 0.2\%$ difference. For the baryons for X_N it is $\lesssim 0.1\%$

ring of the baryon octet³ we have

$$M^2(aab) = M_{0N}^2 + A_1(2\delta m_a + \delta m_b) + A_2(\delta m_b - \delta m_a) + O((\delta m_q)^2). \quad (16)$$

All the expansion coefficients are functions of \bar{m} . It is easy to check that this means that $X_S^2 = M_{0S}^2 + O((\delta m_l)^2)$, $S = \pi, \rho$ and N in agreement with eq. (10).

‘Fan’ plots from the symmetric point down to the physical point are well described by the linear behaviour of eqs. (15) and (16) as shown in [15, 16, 19, 20] which further supports the earlier statement that X_S is constant over a large quark mass range.

Although in our extrapolations, we shall not be using chiral perturbation theory, χ PT, it is natural to ask about its relationship to the $SU(3)$ flavour breaking expansion. This also allows a check on eq. (10), assuming we are in a region where χ PT is valid. This was investigated in [15, 16] for hadron mass singlets and we now extend the argument to t_0 (and w_0), using the result of [21]. Using the notation of this paper and for mass degenerate u and d quark masses we find

$$t_0 = T(\bar{\chi}) \left[1 + \frac{1}{(4\pi f_0)^4} \left(\frac{5}{6}k_2 + \frac{1}{4}k_5'' \right) (\chi_s - \chi_l)^2 + \dots \right], \quad (17)$$

where

$$T(\bar{\chi}) = t_{0,\text{ch}} \left[1 + \frac{3k_1}{(4\pi f_0)^2} \bar{\chi} + \frac{8k_2}{(4\pi f_0)^4} \bar{\chi}^2 \ln \frac{\bar{\chi}}{\Lambda^2} + \frac{9k_4'}{(4\pi f_0)^4} \bar{\chi}^2 \right] \quad (18)$$

being the value of t_0 on the symmetric line ($t_{0,\text{ch}}$ is the value in the chiral limit). k_i are constants, f_0 the pion decay constant again in the chiral limit and $\chi_l = B_0 m_l$, $\chi_s = B_0 m_s$, $\bar{\chi} = \frac{1}{3}(2\chi_l + \chi_s)$.

As expected, there is no linear term, and the first term we see is quadratic in the $SU(3)$ breaking. Further details are given in Appendix A.

4 Lattice matters

4.1 General

We consider 2+1 non-perturbatively $O(a)$ improved clover fermions, as described in [17]. The relation between the bare quark masses m_q in lattice units and the lattice mass parameters κ_q is given by [15, 16]

$$m_q = \frac{1}{2} \left(\frac{1}{\kappa_q} - \frac{1}{\kappa_{0c}} \right) \quad \text{with } q \in \{l, s, 0\}, \quad (19)$$

³For non-degenerate u and d quark mass, the Lambda and Sigma particles mix. This mixing is however very small. This was investigated in [20], where using the notation there, it was shown that $\frac{1}{2}(M_{\Lambda^0}^2 + M_{\Sigma^0}^2) = P_{A_1} = M_{0N}^2 + O((\delta m_q)^2)$, i.e. again we have no linear term in the quark mass. Note also that when the u and d quark masses are degenerate, then no mixing occurs.

β	V	κ_0	κ_l	κ_s	$M_\pi L$	L [fm]
5.80	$48^3 \times 96$	0.122760	0.122760	0.122760	6.95	2.82
5.80	$48^3 \times 96$	0.122810	0.122810	0.122810	6.11	2.82
5.80	$48^3 \times 96$	0.122810	0.122880	0.122670	5.11	2.82
5.80	$48^3 \times 96$	0.122810	0.122940	0.122551	4.01	2.82
5.80	$48^3 \times 96$	0.122870	0.122870	0.122870	4.96	2.82

Table 2: Parameters for $\beta = 5.80$. Each block has the same κ_0 , i.e. constant \overline{m} .

β	V	κ_0	κ_l	κ_s	$M_\pi L$	L [fm]
5.65	$32^3 \times 64$	0.121975	0.121975	0.121975	4.99	2.19
5.65	$32^3 \times 64$	0.122005	0.122005	0.122005	4.67	2.19
5.65	$32^3 \times 64$	0.122005	0.122078	0.121859	4.00	2.19
<i>5.65</i>	$32^3 \times 64$	<i>0.122005</i>	<i>0.122130</i>	<i>0.121756</i>	<i>3.44</i>	<i>2.19</i>
5.65	$32^3 \times 64$	0.122030	0.122030	0.122030	4.32	2.19
5.65	$32^3 \times 64$	0.122050	0.122050	0.122050	4.03	2.19

Table 3: Parameters for $\beta = 5.65$. The entries in italics have $M_\pi L < 4$.

where in simulations we have mass degenerate u and d quarks, i.e. $m_u = m_d \equiv m_l$ and the s quark has mass m_s . Along the $SU(3)$ flavour mass degenerate line, the common quark mass is denoted by m_0 (or equivalently by κ_0) and where vanishing of the quark mass along this line determines κ_{0c} . Along the $\overline{m} = m_0 = \text{constant}$ line gives from eqs. (6) and (19) the $SU(3)$ flavour breaking mass parameter as

$$\delta m_q = \frac{1}{2} \left(\frac{1}{\kappa_q} - \frac{1}{\kappa_0} \right). \quad (20)$$

We see that κ_{0c} has dropped out of this equation, so we do not need its explicit value here. Along this trajectory the choice of quark masses is restricted and we have

$$\kappa_s = \frac{1}{\frac{3}{\kappa_0} - \frac{2}{\kappa_l}}, \quad (21)$$

so once we have decided on a κ_0 , then a given κ_l determines κ_s .

We consider four beta values $\beta = 5.8, 5.65, 5.50, 5.40$ (where $\beta = 10/g_0^2$ with our conventions). In Tables 2, 3, 4 and 5 we give parameters of the runs. The entries in italics have $M_\pi L < 4$.

For example we consider $\beta = 5.50$ on $32^3 \times 64$ lattices with degenerate quark masses of $\kappa_0 = 0.120900, 0.120920, 0.120950$ and 0.120990 which, as we will see, encompasses the initial $SU(3)$ flavour symmetric point on the constant \overline{m} trajectory to the physical point. As can be seen for some of the κ_0 values we have

β	V	κ_0	κ_l	κ_s	$M_\pi L$	L [fm]
5.50	$32^3 \times 64$	0.120900	0.120900	0.120900	5.59	2.37
5.50	$32^3 \times 64$	0.120900	0.121040	0.120620	4.32	2.37
<i>5.50</i>	$32^3 \times 64$	<i>0.120900</i>	<i>0.121095</i>	<i>0.120512</i>	<i>3.72</i>	<i>2.37</i>
<i>5.50</i>	$32^3 \times 64$	<i>0.120900</i>	<i>0.121145</i>	<i>0.120413</i>	<i>3.10</i>	<i>2.37</i>
5.50	$48^3 \times 96$	0.120900	0.121166	0.120371	4.10	3.55
5.50	$32^3 \times 64$	0.120920	0.120920	0.120920	5.27	2.37
5.50	$32^3 \times 64$	0.120920	0.121050	0.120661	4.10	2.37
5.50	$32^3 \times 64$	0.120950	0.120950	0.120950	4.83	2.37
5.50	$32^3 \times 64$	0.120950	0.121040	0.120770	3.97	2.37
<i>5.50</i>	$32^3 \times 64$	<i>0.120950</i>	<i>0.121099</i>	<i>0.120653</i>	<i>3.24</i>	<i>2.37</i>
5.50	$32^3 \times 64$	0.120990	0.120990	0.120990	4.11	2.37

Table 4: Parameters for $\beta = 5.50$.

β	V	κ_0	κ_l	κ_s	$M_\pi L$	L [fm]
5.40	$24^3 \times 48$	0.119860	0.119860	0.119860	4.98	1.96
5.40	$24^3 \times 48$	0.119895	0.119895	0.119895	4.54	1.96
5.40	$24^3 \times 48$	0.119930	0.119930	0.119930	4.11	1.96
<i>5.40</i>	$24^3 \times 48$	<i>0.119930</i>	<i>0.120048</i>	<i>0.119695</i>	<i>3.35</i>	<i>1.96</i>
<i>5.40</i>	$24^3 \times 48$	<i>0.120000</i>	<i>0.120000</i>	<i>0.120000</i>	<i>3.25</i>	<i>1.96</i>

Table 5: Parameters for $\beta = 5.40$.

extended the constant $\overline{m} = m_0$ trajectories down in the direction of the physical point.

While changing the β value gives the greatest change to the singlet terms, smaller effects occur on the $SU(3)$ flavour symmetric line as we change m_0 . This will help us to locate the initial κ_0 , the starting point for the trajectory in the $m_s - m_l$ plane leading to the physical point. Note that if \overline{m} is held constant, then a further advantage of this condition is that for clover fermions the $O(a)$ improved coupling constant remains unchanged as

$$\tilde{g}_0^2 = g_0^2(1 + b_g(g_0)a\overline{m}), \quad (22)$$

although this is unlikely to lead to any large effect.

For orientation the $SU(3)$ symmetric point has a pion mass of about ~ 450 MeV and we reach down to about ~ 260 MeV.

The specific components used in the flow discretisation here are⁴

(f[low], g[auge action], o[bservable])

⁴The flow Wilson action here means $S_{\text{flow}}[U] = \sum \text{Re Tr}[1 - U^{\text{plaq}}]$.

$$= (\text{W[ilson]}, \text{S[ymanzik [tree level]}], \text{C[lover]}) , \quad (23)$$

and the Runge-Kutta discretisation is used for the flow equation, [2].

One can improve the scaling behaviour, which is expected to have $O(a^2)$ corrections. For example for $\sqrt{t_0}$ following [11] we can write

$$\left. \frac{F(t)}{1 + C_2 \frac{a^2}{t} + \dots} \right|_{t=t_{0\text{imp}(c)}} = c \quad \Rightarrow \quad t_{0\text{imp}} = t_0 \left(1 + C_2 \frac{F_0}{F'_0} \frac{a^2}{t_0} + \dots \right) . \quad (24)$$

Inverting this and relabelling $t_{0\text{imp}} \rightarrow t_{0\text{cont}}$ gives

$$t_0 = t_{0\text{cont}} \left(1 - C_2 \frac{F_{0\text{cont}}}{F'_{0\text{cont}}} \frac{a^2}{t_{0\text{cont}}} + \dots \right) , \quad (25)$$

where $F_x = F(t_x)$, $F'_x = t dF(t)/dt|_{t_x}$, with $x \equiv 0$ or 0cont . At tree level for the case here $(fgo) = (WSC)$, $C_2 = -7/72$ [18] so we expect the gradient to be +ve.

4.2 Singlet quantities

We first investigate the constancy of the singlet quantities X_S^2 , as discussed in section 2. In Fig. 2 and 3 we plot X_S^2 for $S = t_0, N, w_0, \rho$ and π against M_π^2/X_π^2

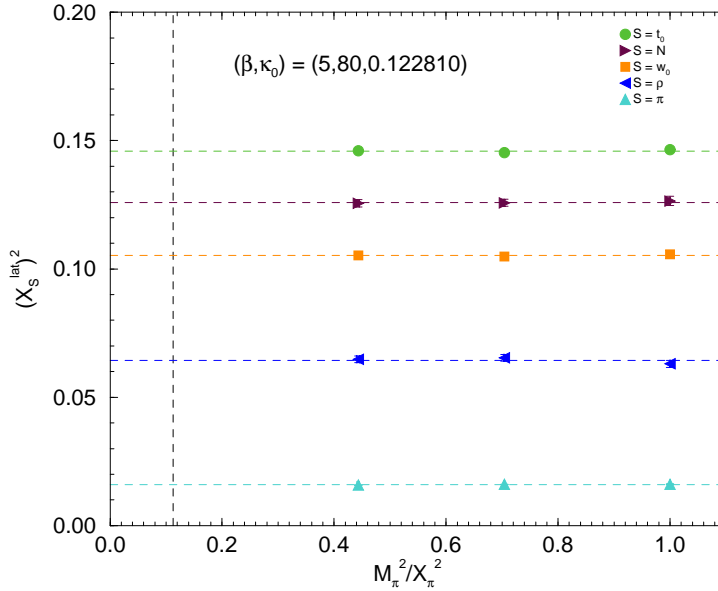


Figure 2: Top to bottom $(X_S^{\text{lat}})^2$ for $S = t_0$ (circles), N (right triangles), w_0 (squares), ρ (left triangles) and π (up triangles) for $(\beta, \kappa_0) = (5.80, 0.122810)$ with constant fits.

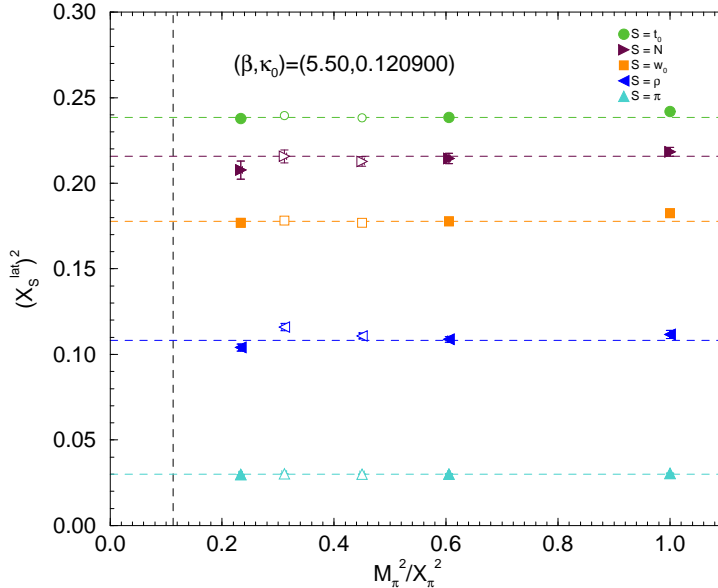


Figure 3: $(X_S^{\text{lat}})^2$ for $S = t_0, N, w_0, \rho$ and π , (top to bottom) for $(\beta, \kappa_0) = (5.50, 0.120900)$ together with constant fits. Same notation as for Fig. 2. Opaque points are not included in the fits, as they have $M_\pi L < 4$.

(which is equivalent to $1/\kappa_l$). The value at $M_\pi^2/X_\pi^2 = 1$ corresponds to the $SU(3)$ symmetric point and the vertical dashed lines correspond to the physical point.

No structure or trend is seen in the results and they are compatible with $(X_S^{\text{lat}})^2$ (and hence X_S^{lat}) a constant down to the vicinity of the physical point. The constant fits exclude points with $M_\pi L < 4$. However these additional points all have $M_\pi L > 3$ and are completely consistent with the fitted points. Thus the constancy of X_S as discussed in sections 2 and 3 is supported by the numerical results.

Furthermore any (significant) quadratic term would mean that each quantity S starts at a slightly different point on the $SU(3)$ flavour symmetric line (but all with the same gradient) and the trajectories would then all focus at the experimental point. We have considered the partially quenched expansion (up to cubic terms in the quark mass) and have determined that along the unitary line considered here these higher order terms are negligible – only when the quark mass is in the vicinity of the charm quark mass do these non-linear terms become appreciable. Thus practically we have a unique starting point on the $SU(3)$ flavour symmetric line for the trajectory to the physical point, i.e. we have the situation for at least $S = t_0, N, w_0, \rho$ and π of the left panel of Fig. 1. To check this an alternative description is provided by a re-arrangement

of $X_\pi^2/X_S^2 = (2M_K^2 + M_\pi^2)/X_S^2$ to give

$$\frac{2M_K^2 - M_\pi^2}{X_S^2} = \frac{X_\pi^2}{X_S^2} - 2\frac{M_\pi^2}{X_S^2}, \quad (26)$$

for $S = N, \rho, t_0, w_0$. So plotting $(2M_K^2 - M_\pi^2)/X_S^2$ against M_π^2/X_S^2 with constant gradient -2 should describe the data for all S . Hence in Fig. 1 left panel the gradient is -2 while for the right panel, we would have an initial gradient of -2 and then some curvature, but all meeting at the physical point.

In Figs. 4 and 5 we present fits of eq. (26) to numerical results of $(2M_K^2 -$

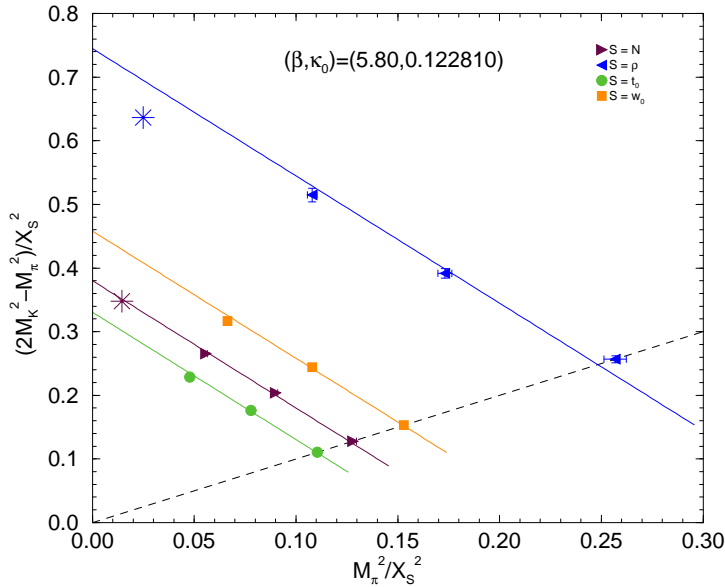


Figure 4: $(2M_K^2 - M_\pi^2)/X_S^2$ against M_π^2/X_S^2 , together with the fit from eq. (26) for $(\beta, \kappa_0) = (5.80, 0.122810)$ and $S = N$ (right triangles), ρ (left triangles), t_0 (circles) and w_0 (squares). The stars correspond to the experimental values for $S = \rho, N$ upper and lower respectively.

$M_\pi^2)/X_S^2$ versus M_π^2/X_S^2 with $S = N, \rho, t_0, w_0$ for the same data sets as in Fig. 2 and 3. Again straight lines (from the fit function) describe the data very well. However as can be seen the lines for the $S = N$ and ρ cases do not quite go through their physical points (denoted by stars). This is because the κ_0 used while close is not quite the value required for the correct path. We shall in future denote this point by κ_0^* . For example, it can be seen that the $\beta = 5.80$, $\kappa_0 = 0.12281$ lines are closer to the physical point, i.e. $\kappa_0 = 0.122810$ is closer to κ_0^* than for the $\beta = 5.50$, $\kappa_0 = 0.120900$ data. Again the picture is best described by the left panel of Fig. 1. So at least for all these quantities we only have to slightly tune to find the appropriate κ_0^* giving the beginning of the path from the $SU(3)$ flavour symmetric line to the physical point.

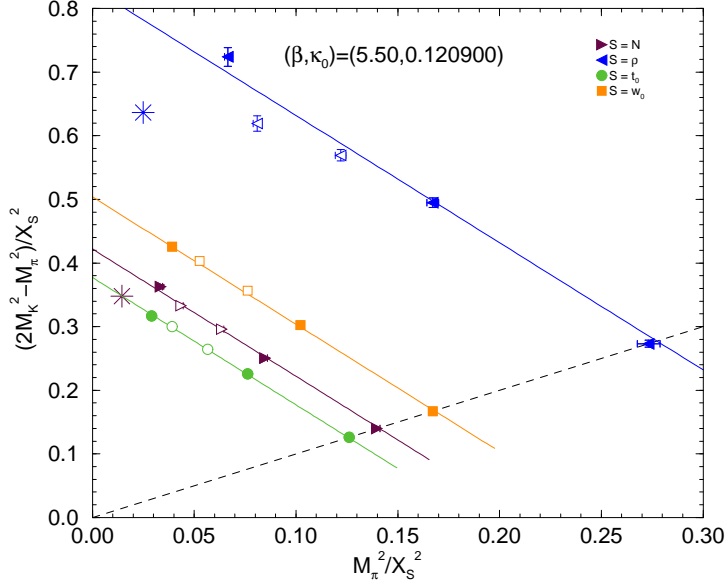


Figure 5: $(2M_K^2 - M_\pi^2)/X_S^2$ against M_π^2/X_S^2 , together with the fit from eq. (26) for $(\beta, \kappa_0) = (5.50, 0.120900)$ and $S = N, \rho, t_0, w_0$. The notation is as for Fig. 4. Opaque points are not included in the fit as they have $M_\pi L < 4$.

5 Scale setting

Using these results we now take $X_S = \text{const.}$ to define the scale, i.e. we set

$$X_S^{\text{lat}} = \text{const.} = a_S X_S^{\text{exp}}. \quad (27)$$

We take the experimental hadron mass results as given in Table 1. As X_{t_0}, X_{w_0} are secondary quantities, i.e. $X_{t_0}^{\text{exp}}, X_{w_0}^{\text{exp}}$ are not experimentally known, they have to be determined.

If we now normalise

$$a_S^2(\kappa_0) = \frac{(X_S^{\text{lat}}(\kappa_0))^2}{(X_S^{\text{exp}})^2}, \quad (28)$$

this provides an estimate for the lattice spacing using the singlet quantity S , which is also a function of the point on the $SU(3)$ flavour symmetric line, i.e. κ_0 (we have indicated this by writing $a_S(\kappa_0)$ for the lattice spacing).

We now vary κ_0 , searching for the location where the various $a_S(\kappa_0)$ cross, providing a value for the common lattice spacing a (and κ_0^*). While ideally we would wish the crossing of all the lines to occur at a single point leading to a common lattice spacing, this, of course, does not quite happen. So we consider pairs of singlet quantities and determine the crossing points, together with the associated (bootstrap) error. In particular we apply this to the pairs

$$(\pi, N), (\pi, \rho). \quad (29)$$

We now use these crossings to adjust X_{t_0} and X_{w_0} so they also go through these points. This determines $\sqrt{t_0^{\text{exp}}}$, w_0^{exp} . For example we have

$$(w_0^{\text{exp}})^2 \equiv \frac{1}{(X_{w_0}^{\text{exp}})^2} = \frac{a^2}{(X_{w_0}^{\text{lat}})^2}. \quad (30)$$

For example in Figs. 6 and 7 we plot $a_S^2(\kappa_0)$ from eq. (28) (in fm^2) against

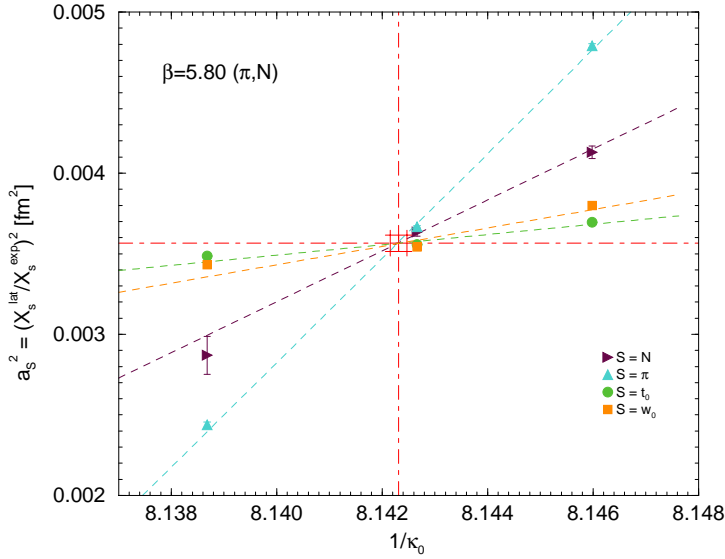


Figure 6: a_S^2 against $1/\kappa_0$ for $S = \pi$ (up triangles), N (right triangles) and t_0 (circles), w_0 (squares) together with linear fits for $\beta = 5.80$.

κ_0 for $\beta = 5.80$ and 5.50 for the singlet quantities $S = \pi$ and N together with $S = t_0$ and w_0 . Where we have three κ_0 values a linear fit in $1/\kappa_0$ is made, while if there are four κ_0 values available then a quadratic fit is made. (However it made very little difference to the later results whether the results from the linear or quadratic fit is used, as mainly interpolations between the X_S^{lat} data is sufficient.) Also plotted is $S = t_0$ and w_0 , again together with appropriate fits. The lattice values have been adjusted with a common factor so these singlet quantities also cross at the same value as (π, N) , which is equivalent to a determination of $\sqrt{t_0^{\text{exp}}}$ and w_0^{exp} as indicated in eq. (30). This procedure is then repeated for the pair (π, ρ) .

For completeness we also take a weighted average of both the (π, N) and (π, ρ) crossings to determine the best $(1/\kappa_0^*, a^2)$. These values are given in Table 6.

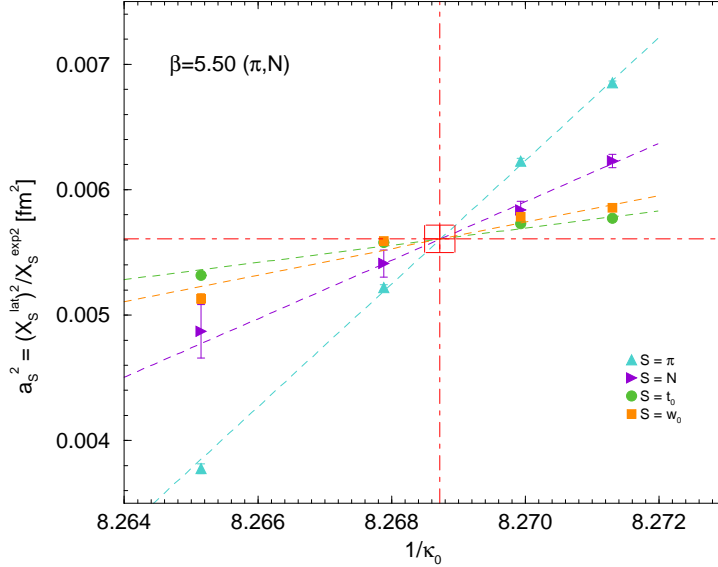


Figure 7: a_s^2 against $1/\kappa_0$ for $S = \pi, N$ and t_0, w_0 together with quadratic fits for $\beta = 5.50$. Notation as for Fig. 6.

β	$1/\kappa_0^*$	a^2 [fm ²]	κ_0^*	a [fm]
5.80	8.14197(12)	0.00346(04)	0.122820(2)	0.0588(03)
5.65	8.19602(15)	0.00468(06)	0.122010(2)	0.0684(04)
5.50	8.26844(13)	0.00547(06)	0.120942(2)	0.0740(04)
5.40	8.33823(25)	0.00669(16)	0.119930(4)	0.0818(09)

Table 6: Determined values of $1/\kappa_0^*$ and a^2 [fm²]. For completeness in the third and fourth columns we also give κ_0^* and a [fm] directly.

6 Continuum results

We are now in a position to perform the last, continuum, extrapolation. In Figs. 8, 9 we show these extrapolations from the pairs (π, N) and (π, ρ) . As anticipated the gradients in a^2 , while small, are positive (c.f. eq. (25)) with the (π, ρ) results being slightly larger than the (π, N) results.

Finally a weighted average from these continuum results (i.e. for $a^2 = 0$) gives our final results

$$\sqrt{t_0^{\text{exp}}} = 0.1511(22)(06)(05)(03) \text{ fm}, \quad w_0^{\text{exp}} = 0.1808(23)(05)(06)(04) \text{ fm}. \quad (31)$$

The first error is statistical, while the second (finite volume), the third ($SU(3)$ flavour breaking expansion) and fourth (scale) are systematic errors as discussed in Appendix B.

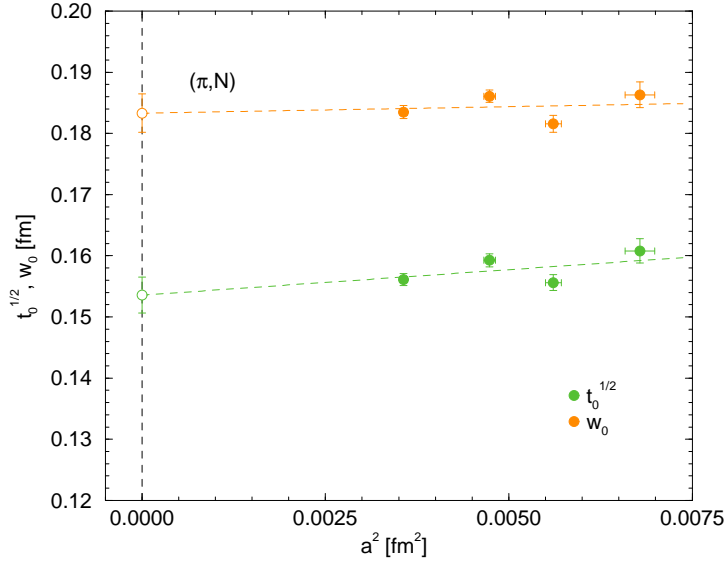


Figure 8: $\sqrt{t_0}$ and w_0 (in fm) against a^2 (in fm²) from the (π, N) crossing together with a linear fit.

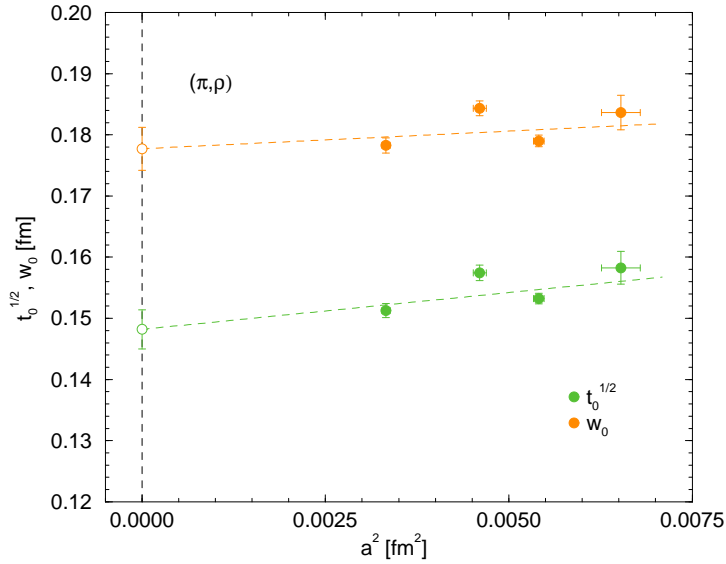


Figure 9: $\sqrt{t_0}$ and w_0 (in fm) against a^2 (in fm²) from the (π, ρ) crossing together with a linear fit.

7 Conclusions

In this article we have described a method for determining the trajectory to approach the physical point, and demonstrated (theoretically and numerically) that singlet quantities remain constant as we approach this point. This enables us by considering pairs of singlet quantities to determine ‘best’ lattice spacings and starting values for the path. By matching these results to the flow variables t_0 and w_0 this enables a determination of their physical values, see eq. (31).

In Fig. 10 we compare these results with other determinations for $n_f = 2 + 1$

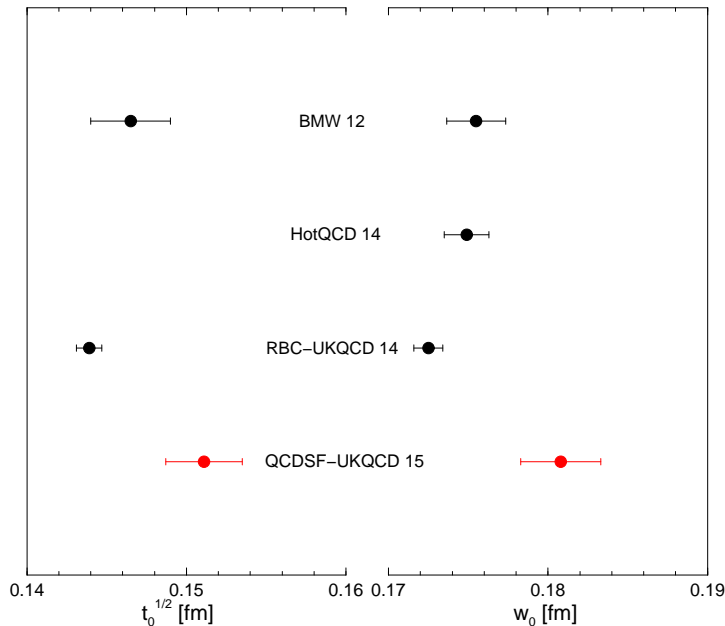


Figure 10: $\sqrt{t_0^{\text{exp}}}$, left panel and w_0^{exp} , right panel in fm for BMW 12 [3], HotQCD 14 [9], RBC-UKQCD 14 [10], together with the present results.

flavours, namely BMW 12 [3], HotQCD 14 [9] and RBC-UKQCD 14 [10]. (The given errors are taken in quadrature.) Reasonable consistency is found between the different determinations.

In conclusion we have determined in this article the flow scales for t_0 and w_0 . These are ‘secondary’ scales and while having the advantage of being cheap and accurate to determine from lattice simulations are not directly experimentally accessible and thus have to be matched to physical quantities.

Acknowledgements

The numerical configuration generation (using the BQCD lattice QCD program [23]) and data analysis (using the Chroma software library [24]) was carried out

on the IBM BlueGene/Q using DIRAC 2 resources (EPCC, Edinburgh, UK), the BlueGene/P and Q at NIC (Jülich, Germany), the Lomonosov at MSU (Moscow, Russia) and the SGI ICE 8200 and Cray XC30 at HLRN (The North-German Supercomputer Alliance) and on the NCI National Facility in Canberra, Australia (supported by the Australian Commonwealth Government). HP was supported by DFG Grant No. SCHI 422/10-1. PELR was supported in part by the STFC under contract ST/G00062X/1 and JMZ was supported by the Australian Research Council Grant No. FT100100005 and DP140103067. We thank all funding agencies.

Appendix

A Singlet chiral perturbation theory: Wilson flow

We want to check that the chiral perturbation theory results for the Wilson flow, as given in [21] are consistent with the $SU(3)$ flavour symmetry expansion [16].

A.1 Pseudoscalar Meson masses

First we need to set out some notation. The quark masses for the $2 + 1$ case are best denoted by χ_q , defined through

$$\begin{aligned}\chi_l &\equiv B_0 m_l \\ \chi_s &\equiv B_0 m_s.\end{aligned}\tag{32}$$

To simplify expressions, it is useful to define some additional χ variables:

$$\begin{aligned}\bar{\chi} &\equiv \frac{1}{3}(2\chi_l + \chi_s) \\ \chi_\pi &\equiv \chi_l \\ \chi_K &\equiv \frac{1}{2}(\chi_s + \chi_l) \\ \chi_\eta &\equiv \frac{1}{3}(2\chi_s + \chi_l),\end{aligned}\tag{33}$$

and a logarithmic function

$$\mu_P \equiv \frac{\chi_P}{(4\pi f_0)^2} \ln \frac{\chi_P}{\Lambda^2} \approx \frac{M_P^2}{(4\pi f_0)^2} \ln \frac{M_P^2}{\Lambda^2}, \quad P \in \pi, K, \eta.\tag{34}$$

In this notation the NLO pseudoscalar meson masses are [22]

$$M_\pi^2 = \chi_\pi \left\{ 1 + q_1 \bar{\chi} + q_2 \chi_\pi + \mu_\pi - \frac{1}{3} \mu_\eta \right\}$$

$$\begin{aligned}
M_K^2 &= \chi_K \left\{ 1 + q_1 \bar{\chi} + q_2 \chi_K + \frac{2}{3} \mu_\eta \right\} \\
M_\eta^2 &= \chi_\eta \left\{ 1 + q_1 \bar{\chi} + q_2 \chi_\eta + 2\mu_K - \frac{4}{3} \mu_\eta \right\} \\
&\quad + \chi_\pi \left\{ -\mu_\pi + \frac{2}{3} \mu_K + \frac{1}{3} \mu_\eta \right\} + q_3 (\chi_s - \chi_l)^2
\end{aligned} \tag{35}$$

where

$$\begin{aligned}
q_1 &= \frac{48}{f_0^2} (2L_6 - L_4) \\
q_2 &= \frac{16}{f_0^2} (2L_8 - L_5) \\
q_3 &= \frac{128}{9f_0^2} (3L_7 + L_8).
\end{aligned} \tag{36}$$

A.2 Wilson Flow scale, t_0

In [21], eq.(4.10), Bär and Golterman give the form expected for the quantity t_0 at NNLO in chiral perturbation theory.

$$\begin{aligned}
t_0 &= t_{0,\text{ch}} \left[1 + \frac{k_1}{(4\pi f_0)^2} (2M_K^2 + M_\pi^2) \right. \\
&\quad + \frac{1}{(4\pi f_0)^2} \left((3k_2 - k_1) M_\pi^2 \mu_\pi + 4k_2 M_K^2 \mu_K + \frac{k_1}{3} (M_\pi^2 - 4M_K^2) \mu_\eta + k_2 M_\eta^2 \mu_\eta \right) \\
&\quad \left. + \frac{k_4}{(4\pi f_0)^4} (2M_K^2 + M_\pi^2)^2 + \frac{k_5}{(4\pi f_0)^4} (M_K^2 - M_\pi^2)^2 \right]
\end{aligned} \tag{37}$$

The free parameters in this expression are k_1, k_2, k_4, k_5 . Most terms in the expression are obviously symmetric, but the k_1 term has been written in a way that obscures its symmetry.

Using eqs. (35) to translate eq. (37) into χ variables⁵

$$\begin{aligned}
t_0 &= t_{0,\text{ch}} \left[1 + \frac{3k_1}{(4\pi f_0)^2} \bar{\chi} + \frac{k_2}{(4\pi f_0)^2} (3\chi_\pi \mu_\pi + 4\chi_K \mu_K + \chi_\eta \mu_\eta) \right. \\
&\quad \left. + \frac{9k'_4}{(4\pi f_0)^4} \bar{\chi}^2 + \frac{k'_5}{4(4\pi f_0)^4} (\chi_s - \chi_l)^2 \right]
\end{aligned} \tag{38}$$

with

$$\begin{aligned}
k'_4 &= k_4 + \frac{1}{3} (4\pi f_0)^2 k_1 (q_1 + q_2) \\
k'_5 &= k_5 + \frac{2}{3} (4\pi f_0)^2 k_1 q_2.
\end{aligned} \tag{39}$$

⁵In this Appendix we work to order χ_q^2 , dropping terms of order χ_q^3 .

The expression in eq. (38) is simpler and more explicitly symmetric than eq. (37).

As usual, we get a further simplification if we restrict ourselves to the line of constant $\bar{\chi}$,

$$t_0 = T \left[1 + \frac{k_2}{(4\pi f_0)^4} \left(3\chi_\pi^2 \ln \frac{\chi_\pi}{\bar{\chi}} + 4\chi_K^2 \ln \frac{\chi_K}{\bar{\chi}} + \chi_\eta^2 \ln \frac{\chi_\eta}{\bar{\chi}} \right) + \frac{k_5''}{4(4\pi f_0)^4} (\chi_s - \chi_l)^2 \right] \quad (40)$$

with

$$k_5'' = k_5' + \frac{20}{9} k_2 \ln \frac{\bar{\chi}}{\Lambda^2} \quad (41)$$

and

$$T = t_{0,\text{ch}} \left[1 + \frac{3k_1}{(4\pi f_0)^2} \bar{\chi} + \frac{8k_2}{(4\pi f_0)^4} \bar{\chi}^2 \ln \frac{\bar{\chi}}{\Lambda^2} + \frac{9k_4'}{(4\pi f_0)^4} \bar{\chi}^2 \right] \quad (42)$$

being the value of t_0 on the symmetric line. We can Taylor expand eq. (40) about the symmetric point, the result is

$$t_0 = T \left[1 + \frac{1}{(4\pi f_0)^4} \left(\frac{5}{6} k_2 + \frac{1}{4} k_5'' \right) (\chi_s - \chi_l)^2 + \dots \right]. \quad (43)$$

As expected, there is no linear term, and the first term we see is quadratic in the $SU(3)$ breaking.

B Systematic errors

We follow here the more general discussion given in Appendix A of [19].

B.1 Finite lattice volume

Clearly the argument given in section 2 that X_S is flat along the $SU(3)$ flavour symmetric point holds for any volume. As discussed in [16] for an estimate of finite volume effects, a suitable expression is given by

$$X_S^2(L) = X_S^2 \left(1 + c_S \frac{1}{3} [f_L(M_\pi) + 2f_L(M_K)] \right). \quad (44)$$

Lowest order χ PT, [25, 26] indicates that reasonable functional forms for $f_L(M)$ are

$$\begin{aligned} f_L(M) &= (aM)^2 \frac{e^{-ML}}{(ML)^{3/2}}, & \text{meson,} \\ f_L(M) &= (aM)^2 \frac{e^{-ML}}{(X_N L)}, & \text{baryon.} \end{aligned} \quad (45)$$

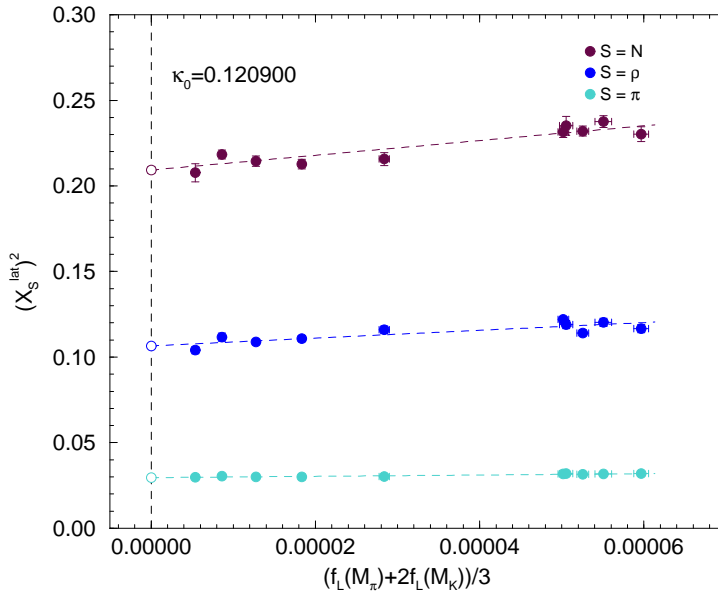


Figure 11: $(X_S^{\text{lat}})^2$ versus $(f_L(M_\pi) + 2f_L(M_K))/3$ for $(\beta, \kappa_0) = (5.50, 0.120900)$, with N (squares), ρ (diamonds) and π (upper triangles). The left-most clusters of points are from the $32^3 \times 64$ and $48^3 \times 96$ lattices, while the right cluster is from $24^3 \times 48$ lattices. The dashed lines are linear fits.

In Fig. 11 we plot $(f_L(M_\pi) + 2f_L(M_K))/3$ against $(X_S^{\text{lat}})^2$ for $S = N, \rho$ and π on $48^3 \times 96$, $32^3 \times 64$ and additionally $24^3 \times 48$ lattices for $\beta = 5.50$ and $\kappa_0 = 0.120900$. The fits are linear, with reasonable agreement to the data. Little finite size effect is seen between the larger lattice volume results used in the previous analysis and the extrapolated value here. For the case considered here for (X_π, X_N, X_ρ) the changes are about (1.3, 2.9, 1.5)%. Taking this as an increase in errors for all the data sets and performing the same analysis gives the change in the central values and errors, taken as the systematic error as given in eq. (31).

B.2 $SU(3)$ flavour breaking expansion

We first note that in Figs. 2, 3 from the $SU(3)$ flavour symmetric line down to the physical point lies in the range $|\delta m_l| \lesssim 0.01$ (and $|\delta m_s| \lesssim 0.02$), e.g. [20] and that mass ‘fan plots’ (e.g. Fig. 5 of [20]) show little curvature. This is in agreement with the $SU(3)$ flavour breaking expansion, eq. (15) or (16). The next order in the expansion is multiplied by a further δm_q . So we expect that every increase in the order leads to a decrease by an order of magnitude or more (often by a factor ~ 20) in the series. So we believe that convergence is very good for hyperons. (Such an expansion is good compared to most approaches available to QCD.) Nevertheless we have, however, made tests with a linear or quadratic

fit for example for the nucleon in Fig. 3 and followed this through the analysis. The final change in central value for $\sqrt{t_0}$ and w_0 was not large, we include it as a (second) systematic error.

B.3 Physical scale

As mentioned in footnote 2 physical values of hadron masses have a small electromagnetic component. Although we disregard this in our analysis, we make a small allowance here, and take $\sqrt{t_0^{\text{exp}}}$, w_0^{exp} to also have a similar error as X_π , i.e. a systematic error of $\sim 0.2\%$ due to electromagnetic effects.

References

- [1] M. Lüscher, *Commun. Math. Phys.* **293** (2010) 899, [arXiv:0907.5491 [hep-lat]].
- [2] M. Lüscher, *JHEP* **071** (2010) 1008, [arXiv:1006.4518 [hep-lat]].
- [3] S. Borsanyi, S. Dürr, Z. Fodor, C. Hoelbling, S. D. Katz, S. Krieg, T. Kurth, L. Lellouch, T. Lippert and C. McNeile, [BMW Collaboration], *JHEP* **010** (2012) 1209, [arXiv:1203.4469 [hep-lat]].
- [4] R. Sommer, *Proc. Sci. LATTICE 2013* (2013) 015, arXiv:1401.3270 [hep-lat].
- [5] M. Asakawa, T. Hatsuda, T. Iritani, E. Itou, M. Kitazawa and H. Suzuki, arXiv:1503.06516 [hep-lat].
- [6] A. Francis, O. Kaczmarek, M. Laine, T. Neuhaus and H. Ohno, *Phys. Rev. D* **91** (2015) 096002, [arXiv:1503.05652 [hep-lat]].
- [7] S. Datta, S. Gupta, A. Lahiri, A. Lytle and P. Majumdar, arXiv:1507.00821 [hep-lat].
- [8] M. Bruno and R. Sommer, *Proc. Sci. LATTICE 2013* (2013) 321, arXiv:1311.5585 [hep-lat].
- [9] A. Bazavov, T. Bhattacharya, C. DeTar, H.-T. Ding, S. Gottlieb, R. Gupta, P. Hegde, U. M. Heller, F. Karsch, E. Laermann, L. Levkova, S. Mukherjee, P. Petreczky, C. Schmidt, C. Schroeder, R. A. Soltz, W. Soeldner, R. Sugar, M. Wagner and P. Vranas, [HotQCD Collaboration], *Phys. Rev. D* **90** (2014) 094503, [arXiv:1407.6387 [hep-lat]].

- [10] T. Blum, P. A. Boyle, N. H. Christ, J. Frison, N. Garron, R. J. Hudspith, T. Izubuchi, T. Janowski, C. Jung, A. Jüttner, C. Kelly, R. D. Kenway, C. Lehner, M. Marinkovic, R. D. Mawhinney, G. McGlynn, D. J. Murphy, S. Ohta, A. Portelli, C. T. Sachrajda and A. Soni, [RBC–UKQCD Collaborations], [arXiv:1411.7017](#) [[hep-lat](#)].
- [11] A. Bazavov, C. Bernard, N. Brown, C. DeTar, J. Foley, S. Gottlieb, U. M. Heller, J. Komijani, J. Laiho, L. Levkova, R. L. Sugar, D. Toussaint and R. S. Van de Water, [MILC Collaboration], [arXiv:1503.02769](#) [[hep-lat](#)].
- [12] R. J. Dowdall, C. T. H. Davies, G. P. Lepage and C. McNeile, *Phys. Rev. D* **88** (2013) 074504, [[arXiv:1303.1670](#)] [[hep-lat](#)].
- [13] A. Deuzeman and U. Wenger, *Proc. Sci. Lattice 2012* (2012) 162.
- [14] R. Horsley, J. Najjar, Y. Nakamura, H. Perlt, D. Pleiter, P. E. L. Rakow, G. Schierholz, A. Schiller, H. Stüben and J. M. Zanotti, [QCDSF–UKQCD Collaborations], *Proc. Sci. LATTICE 2013* (2013) 249, [arXiv:1311.5010](#) [[hep-lat](#)].
- [15] W. Bietenholz, V. Bornyakov, N. Cundy, M. Göckeler, R. Horsley, A. D. Kennedy, W. G. Lockhart, Y. Nakamura, H. Perlt, D. Pleiter, P. E. L. Rakow, A. Schäfer, G. Schierholz, A. Schiller, H. Stüben and J. M. Zanotti, [QCDSF–UKQCD Collaboration], *Phys. Lett. B* **690** (2010) 436, [[arXiv:1003.1114](#)] [[hep-lat](#)].
- [16] W. Bietenholz, V. Bornyakov, M. Göckeler, R. Horsley, W. G. Lockhart, Y. Nakamura, H. Perlt, D. Pleiter, P. E. L. Rakow, G. Schierholz, A. Schiller, T. Streuer, H. Stüben, F. Winter and J. M. Zanotti, [QCDSF–UKQCD Collaboration], *Phys. Rev. D* **84** (2011) 054509, [[arXiv:1102.5300](#)] [[hep-lat](#)].
- [17] N. Cundy, M. Göckeler, R. Horsley, T. Kaltenbrunner, A. D. Kennedy, Y. Nakamura, H. Perlt, D. Pleiter, P. E. L. Rakow, A. Schäfer, G. Schierholz, A. Schiller, H. Stüben and J. M. Zanotti, [QCDSF–UKQCD Collaboration], *Phys. Rev. D* **79** (2009) 094507, [[arXiv:0901.3302](#)] [[hep-lat](#)].
- [18] Z. Fodor, K. Holland, J. Kuti, S. Mondal, D. Negradi and C. H. Wong, *JHEP* **1409** (2014) 018, [[arXiv:1406.0827](#)] [[hep-lat](#)].
- [19] R. Horsley, J. Najjar, Y. Nakamura, D. Pleiter, P. E. L. Rakow, G. Schierholz and J. M. Zanotti, [QCDSF–UKQCD Collaboration], *Phys. Rev. D* **86** (2012) 114511, [[arXiv:1206.3156](#)] [[hep-lat](#)].
- [20] R. Horsley, J. Najjar, Y. Nakamura, H. Perlt, D. Pleiter, P. E. L. Rakow, G. Schierholz, A. Schiller, H. Stüben and J. M. Zanotti, [QCDSF–UKQCD Collaboration], *Phys. Rev. D* **91** (2015) 074512, [[arXiv:1411.7665](#)] [[hep-lat](#)].

- [21] O. Bär and M. Golterman, *Phys. Rev.* **D89** (2014) 034505, [arXiv:1312.4999[hep-lat]].
- [22] J. Gasser and H. Leutwyler, *Nucl. Phys.* **B250** (1985) 465.
- [23] Y. Nakamura and H. Stüben, *Proc. Sci. Lattice 2010* (2010) 040, arXiv:1011.0199[hep-lat].
- [24] R. G. Edwards and B. Joó, *Nucl. Phys. Proc. Suppl.* **140** (2005) 832, arXiv:hep-lat/0409003.
- [25] G. Colangelo, S. Dürr and C. Haefeli, *Nucl. Phys.* **B721** (2005) 136 [arXiv:hep-lat/0503014].
- [26] A. Ali Khan, T. Bakeyev, M. Göckeler, T. R. Hemmert, R. Horsley, A. C. Irving, B. Joó, D. Pleiter, P. E. L. Rakow, G. Schierholz and H. Stüben, [QCDSF–UKQCD Collaboration], *Nucl. Phys.* **B689** (2004) 175 [arXiv:hep-lat/0312030].